J. Appl. Comput. Mech., 6(4) (2020) 1012-1029
DOI: 10.22055/JACM.2019.30095.1678

ISSN: 2383-4536
jacm.scu.ac.ir

M&MoCS

Shahid Chamran University of Ahvaz

Journal of Applied and Computational Mechanics

Research Paper

Three Dimensional Non-linear Radiative Nanofluid Flow over a Riga Plate

A.K. Abdul Hakeem[1], P. Ragupathi[1], S. Saranya[1], B. Ganga[2]

[1] Department of Mathematics, Sri Ramakrishna Mission Vidyalaya College of Arts and Science, Coimbatore - 641 020, India
[2] Department of Mathematics, Providence College for Women, Coonoor - 643 104, India

Received June 27 2019; Revised September 13 2019; Accepted for publication September 15 2019.
Corresponding author: A.K. Abdul Hakeem (abdulhakeem6@gmail.com)

Abstract. Numerous techniques in designing zones happen at high temperature and functions under high temperature are in a way that involves non-linear radiation. In weakly conducting fluids, however, the currents induced by an external magnetic field alone are too small, and an external electric field must be applied to achieve an efficient flow control. Gailitis and Lielausis, devised Riga plate to generate a crossed electric and magnetic fields which can produce a wall parallel Lorentz force in order to control the fluid flow. It acts as an efficient agent to reduce the skin friction. So, in this paper, we start the numerical investigation on the three-dimensional flow of nanofluids with the inclusion of non-linear radiation past a Riga plate. To this end, the numerical investigation is conducted on the three-dimensional flow of nanofluids with the inclusion of non-linear radiation past a Riga plate. Water (H_2O) and Sodium Alginate ($NaC_6H_9O_7$) are the base fluids, whereas Magnetite (Fe_3O_4) and Aluminium oxide (Al_2O_3) are the nanoparticles. The mathematical formulation for Sodium Alginate base fluid is separated through the Casson model. Suitable transformations on governing partial differential equations yield strong non-linear ordinary differential equations. Numerical solutions for the renewed system are constructed by fourth-order Runge-Kutta method with shooting technique. Various deductions for flow and heat transfer attributes are sketched and discussed for various physical parameters. Furthermore, the similarities with existing results were found for the physical quantities of interest. It was discovered, that the temperature ratio parameter and the radiation parameter enhance the rate of heat transport. Moreover, the $NaC_6H_9O_7$ - Al_2O_3 nanofluid improves the heat transfer rate. Likewise, H_2O-Fe_3O_4 nanofluid stimulates the local skin friction coefficients.

Keywords: Non-linear radiation; Riga plate; Three-dimensional flow; Nanofluid; Nanoparticles.

1. Introduction

Today, the collaboration of thermal radiation with forced convection assumes a central part in numerous realistic applications. Specifically, applications like power plants using nuclear energy, aircraft, self-propelled nuclear explosives, the processes that involve fast moving flow of the gas over a wheel for producing continuous power, the pushing devices in the space vehicles, and so on, depending upon the radiative heat transfer. Thus, the thermal radiation influenced many researchers to participate in establishing its effectiveness under various conditions. Ghadikolaei et al. [1] analyzed the natural convection MHD flow due to $MoS_2 - Ag$ nanoparticles suspended in $C_2H_6O_2 - H_2O$ hybrid base fluid with thermal radiation. Also, he investigated the terrific effect of H_2 on 3D free convection MHD flow of $C_2H_6O_2 - H_2O$ hybrid base fluid to dissolve Cu nanoparticles in a porous space considering the thermal radiation and nanoparticle shape effects [2]. Numerical simulation for impact of Coulomb force on nanofluid heat transfer in a porous enclosure in the

Published online: November 30 2019

presence of thermal radiation was examined by Sheikholeslami and Rokni [3]. More interesting discussion on thermal radiation can be found from [4-7]. In order to replicate the physiological effects of radiation, Rosseland approximation was put into use. Moreover, they took the smallest temperature variations in the flow of radiation incident on an area in a given time, however, during the time that the dissimilarity across the space beginning from the sheet to the surrounding temperature is high, evoked the importance of non-linear radiation. Factories that function under high temperature are closely connected with non-linear radiation. Therefore, for which showcased their interest. Quite a lot of advances targeting MHD serve as the basis for the examinations [8-19].

Being dispersed throughout in various base fluids, the nanoparticles can revise the characteristics of the normal heat transfer fluids. This creative composition was given a particular name, nanofluids by Choi [20]. The potency of metal as measured by the amount was three times the measure of strength needed to produce thermal conductivities by a normal fluid. This new context of microscopic metallic particles with the base fluids presented an incredible upgrade in the liquids thermophysical condition. All the way, nanofluids in different modern procedures involving nano-tech, for example, avoiding electronic gadgets to become hot, controlling vehicle warm up, atomic reactor and numerous others. At that point, a numerical model was broken down by Buongiorno [21] for the stream of nanofluids which were to predict the attributes of thermophoresis and erratic random movement of microscopic particles. Sheikholeslami [22] carried out a numerical inquiry on the water-based Al_2O_3 nanofluid flow inside a permeable medium employing an innovative computer method. The information about the nanofluid streams is currently very largish. Be that as it may, the couple of late examinations toward this path can be seen through the works [23-37]. An act of assessing non-Newtonian liquids has been the latest progress in fluid mechanics, playing an essential part in a few modern applications. The possibility of heat transfer improvement in diverse progressions was assessed with the conduct of non-Newtonian liquid. In perspective of the miscellaneous peculiarity of non-Newtonian liquids in the environment, analysts [38-42] looked over a selection of non-Newtonian liquids showing signs of unlike nature. A model of 3D was adopted for a Casson nanofluid of which it is assumed to move steadily above a porous linearly extending sheet introducing convection typically near the surface was subjected to examination by Mahanta and Shaw [43]. Butt et al. [44] studied the same formulation for an unsteady stretching sheet. With that Shehzad et al. [45] added his work for heat generation effects. As a part of this collection, comprising the works of Nadeem et al. [46], Yousif et al. [47] and Gireesha et al. [48].

In contrast, an association between the electrodes and magnets that are alternately arranged into their appropriate relative positions above a completely flat surface, acknowledged being the Riga plate can be useful in diminishing drag by putting a stop to boundary layer separation. Owing to these purposes theoretical plus experimental survey has been done by various specialists on Riga plate. For instance, Hayat et al. [49], Ahmad et al. [50], Abbas et al. [51], Hayat et al. [52], Ahmad et al. [53] and Mahanthesh et al. [54].

Recently, Ganesh Kumar et al. [57] studied the flow behavior of Prandtl liquid over a flat plat. Motivated from this path uncovers that, so far no one has considered to build up a mathematical model for comparing the effects of non-linear radiation in the three-dimensional flow of $H_2O/NaC_6H_9O_7$ base fluids with Fe_3O_4/Al_2O_3 nanoparticles over a Riga plate. Consequently, from the gathered information the present study incorporates some new aspects, which happens to be the novelties of this study and are listed below.

- Nanofluid in 3D flow was introduced.
- Fe_3O_4 and Al_2O_3 nanoparticles was suspended within Water and Sodium Alginate base fluids.
- Non-linear radiation was taken into account.
- Riga plate was implemented, which induces the flow.
- Results in the absence of nanoparticles when compared with Ganesh Kumar et al. [57], Wang [56], and Hayat et al. [55] was in good agreement.

Also, the important observations of investigation are the temperature ratio parameter and the radiation parameter enhance the rate of heat transport, the $NaC_6H_9O_7-Al_2O_3$ nanofluid improves the heat transfer rate. Likewise, $H_2O-Fe_3O_4$ nanofluid stimulates the local skin friction coefficients.

2. Mathematical Formulation

We consider a steady, three-dimensional flow of incompressible $H_2O/NaC_6H_9O_7$ base fluids with Fe_3O_4/Al_2O_3 nanoparticles. The Riga plate is employed at $z=0$ to induce the flow. The plate kept at the $xv-$ plane where $z=0$ and the flow is assumed to occur in the $z>0$ domain. Let $u=U_w(x)=ax$ and $v=V_w(y)=by$ be the stretching velocities of the Riga plate along $x-$ and $y-$ directions respectively. Also, we assume that the rheological state for an incompressible Casson fluid can be written be written as :(for more details see [29])

Table 1. Thermophysical properties of H_2O and $NaC_6H_9O_7$ base fluids and Fe_3O_4 and Al_2O_3 nanoparticles [23]

	ρ $(Kg\,m^{-3})$	C_p $(J\,Kg^{-1}\,K^{-1})$	k $(Wm^{-1}\,K^{-1})$
Water	997	4179	0.613
Sodium Alginate	989	4175	0.6376
Magnetite	5180	670	9.7
Aluminium Oxide	3970	765	40

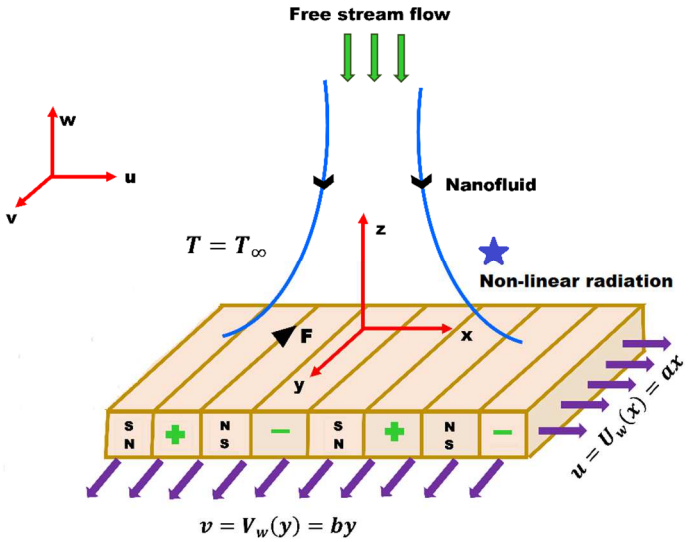

Fig. 1. Geometrical representation of the problem

$$\tau = \tau_0 + \mu\gamma^* \tag{1}$$

$$\tau_{ij} = \begin{cases} 2\left(\dfrac{\sqrt{2\Pi}\mu_B + p_y}{\sqrt{2\Pi}}\right)e_{ij}, \Pi_c < \Pi \\ 2\left(\dfrac{\sqrt{2\Pi}_c\mu_B + p_y}{\sqrt{2\Pi}_c}\right)e_{ij}, \Pi_c > \Pi \end{cases} \tag{2}$$

The governing boundary layer equations of momentum and energy for three-dimensional flow can be written as: [11, 57].

$$\frac{\partial u}{\partial x} + \frac{\partial v}{\partial y} + \frac{\partial w}{\partial z} = 0 \tag{3}$$

$$u\frac{\partial u}{\partial x} + v\frac{\partial u}{\partial y} + w\frac{\partial u}{\partial z} = \nu_{nf}\left(1 + \frac{1}{\beta}\right)\frac{\partial^2 u}{\partial z^2} + \frac{\pi j_0 M_0}{8\rho_{nf}}e^{\left(\frac{-\pi}{a_1}z\right)} \tag{4}$$

$$u\frac{\partial v}{\partial x} + v\frac{\partial v}{\partial y} + w\frac{\partial v}{\partial z} = \nu_{nf}\left(1 + \frac{1}{\beta}\right)\frac{\partial^2 v}{\partial z^2} \tag{5}$$

$$u\frac{\partial T}{\partial x} + v\frac{\partial T}{\partial y} + w\frac{\partial T}{\partial z} = \alpha_{nf}\frac{\partial^2 T}{\partial z^2} - \frac{1}{\left(\rho C_p\right)_{nf}}\frac{\partial q_r}{\partial z} \tag{6}$$

where u, v and w are the x, y and z components of velocity, β is the Casson parameter. ν_{nf} is the kinematic viscosity of the nanofluid, ρ_{nf} is the density of the nanofluid, $\left(C_p\right)_{nf}$ is the specific heat capacity of the nanofluid, j_0 is the current density applied to the electrodes, M_0 is the magnetic property of the permanent magnets that are organized on top of the plate surface, a_1 denotes the diameter of the magnets positioned in the interval separating the electrodes and ϕ is the particle of volume fraction. The radiative heat flux terms are simplified by using Rosseland diffusion approximation (Saranya et al. [11]) and accordingly:

$$q_r = \frac{-16\sigma^* T_\infty^3}{3k^*}\frac{\partial T}{\partial z} \tag{7}$$

where σ^* is the Stefan-Boltzmann and k^* is the mean absorption coefficient. In view to Eq. (7), energy Eq. (6) will take the form:

$$u\frac{\partial T}{\partial x}+v\frac{\partial T}{\partial y}+w\frac{\partial T}{\partial z}=\frac{\partial}{\partial z}\left[\left(\alpha_{nf}+\frac{16\sigma^{*}T_{\infty}^{3}}{3k^{*}\left(\rho C_{p}\right)_{nf}}\right)\frac{\partial T}{\partial z}\right] \tag{8}$$

The boundary conditions for the present flow analysis are:

$$\begin{aligned} &u=U_w(x), v=V_w(y), w=0, T=T_w, \ at \quad z=0\\ &u\to 0, \ v\to 0, \ T\to T_\infty \qquad as \ \ z\to\infty \end{aligned} \tag{9}$$

where the fluid temperature of the wall is T_w.

$$\begin{aligned} &\eta=z\sqrt{\frac{a}{\nu_f}}, u=axf'(\eta), v=ayg'(\eta),\\ &w=-\sqrt{a\nu_f}\left(f(\eta)+g(\eta)\right), \theta(\eta)=\frac{T-T_\infty}{T_w-T_\infty} \end{aligned} \tag{10}$$

The similarity transformations stated in Eq. (10) automatically is satisfies Eq. (3) and Eqs. (4), (5) and (8) becomes:

$$\left(\beta^{-1}(\beta+1)\right)A_1 f'''+(f+g)f''-f'^{2}+QA_2e^{-\eta A}=0 \tag{11}$$

$$(\beta^{-1}(\beta+1))A_1 g'''+(f+g)g'-g'^{2}=0 \tag{12}$$

$$A_4+Rd\left(1+(\theta_w-1)\theta\right)^{3}\theta''+\Pr A_3(f+g)\theta'=0 \tag{13}$$

The transformed boundary conditions are:

$$\begin{aligned} &f=0, g=0, f'=1, g=\alpha, \theta=1 \ \ at \ \ \eta=0\\ &f'\to 0, g'\to 0, \ \theta\to 0 \ \ as \ \ \eta\to\infty \end{aligned} \tag{14}$$

where, $A_1=1/[(1-\varphi)^{2.5}](1-\varphi+\varphi[\rho_s/\rho_f])$, $A_2=1/(1-\varphi+\varphi[\rho_s/\rho_f])$, $A_3=(1-\varphi+\varphi[(\rho C_p)_s/(\rho C_p)_f])$, $A_4=k_{nf}/k_f$, $\alpha=b/a$ is the stretching ratio parameter, $\Pr=\mu_f(C_p)_f/k_f$ is the Prandtl number, $Q=\pi j_0 M_0 x/8\rho_f U_w^2$ is the modified Hartmann number and $A=\pi/a_1(a/\nu)^{-1/2}$ is the dimensionless parameter, $\theta_w\left(=T_w/T_\infty\right)$ is temperature ratio parameter, $Rd=16\sigma^{*}T_\infty^3/3k_f k^{*}$ is the radiation parameter.

If $C_{fx}Re_x^{0.5}$ and $C_{fy}Re_y^{0.5}$ are the local skin-friction coefficients and $Nu_x Re_x^{-0.5}$ is the local Nusselt number, then we have (see Ghadikolaei et al. [30])

$$C_{fx}\,\mathrm{Re}_x^{0.5}=\frac{\tau_w x}{\rho_f u_w^2}, C_{fy}\,\mathrm{Re}_y^{0.5}=\frac{\tau_w y}{\rho_f u_w^2}, Nu_x\,\mathrm{Re}_x^{-0.5}=\frac{xq_w}{k_f\left(T_w-T_\infty\right)} \tag{15}$$

Table 2. Applied formulation of nanofluids properties ([42])

Nanofluid properties	Applied model
Density	$\rho_{nf}=(1-\phi)\rho_f+\rho_s$
Thermal diffusivity	$\alpha_{nf}=\frac{k_{nf}}{\left(\rho C_p\right)_{nf}}$
Heat capacitance	$\left(\rho C_p\right)_{nf}=(1-\phi)\left(\rho C_p\right)_f+\left(\rho C_p\right)_s$
Kinematic viscosity	$\nu_{nf}=\frac{\mu_{nf}}{\rho_{nf}}$
Dynamic viscosity	$\mu_{nf}=\frac{\mu_f}{(1-\phi)^{2.5}}$
Thermal conductivity	$\frac{k_{nf}}{k_f}=\frac{k_s+2k_f-2\phi\left(k_f-k_s\right)}{k_s+2k_f+\phi\left(k_f-k_s\right)}$

where τ_w and q_w are the wall shear stress and the wall heat flux, respectively. The above equation in dimensionless form can be written as:

$$\begin{aligned} Re_x^{0.5} C_{fx} &= (1-\phi)^{-2.5}(\beta^{-1}(\beta+1)) f''(0), \\ Re_x^{0.5} C_{fy} &= \alpha^{-3/2}(1-\phi)^{-2.5}(\beta^{-1}(\beta+1)) g''(0) \\ Re_x^{-0.5} Nu_x &= -(A_4 + Rd(\theta_w)^3)\theta'(0) \end{aligned} \tag{16}$$

where the definition of Reynold's number is $\mathrm{Re} = U_w(x)x/\nu_f$ and $\mathrm{Re} = V_w(y)y/\nu_f$.

Table 3. Comparison of results of different value of α with Wang [56], Hayat et al. [55] and Ganesh Kumar et al. [57]

	Wang [56]		Hayat et al. [55]		Ganesh Kumar et al. [57]		Present Result	
α	$-f''(0)$	$-g''(0)$	$-f''(0)$	$-g''(0)$	$-f''(0)$	$-g''(0)$	$-f''(0)$	$-g''(0)$
0	1	0	1	0	1	0	1.00000000	0
0.25	1.0488	0.1945	1.048810	0.19457	1.04906	0.19457	1.04881108	0.19456383
0.5	1.0930	0.4652	1.093095	0.465205	1.09324	0.46532	1.09309502	0.46520485
0.75	1.1344	0.7946	1.134500	0.794620	1.13458	0.79470	1.13448575	0.79461826
1	1.1737	1.1737	1.173721	1.173721	1.17378	1.17378	1.17372074	1.17372074

3. Numerical Solution

It is tough dealing with the solutions for the highly non-linear equations (11) - (13) analytically. This difficult situation is dealt numerically by assisting R-K method as well as shooting technique. For the usage of R-K method, the boundary value problems must be transformed into an initial value problem. Starting with initial conditions, the increment in the converted equations are computed by means of the following formula:

$$\begin{aligned} k_1 &= h f_1(x_0, y_0) \\ k_2 &= h f_1\left(x_0 + \frac{h}{2}, y_0 + \frac{k_1}{2}\right) \\ k_3 &= h f_1\left(x_0 + \frac{h}{2}, y_0 + \frac{k_2}{2}\right) \\ k_4 &= h f_1(x_0 + h, y_0 + k_3) \\ \Delta y &= \frac{k_1 + 2k_2 + 2k_3 + k_4}{6} \end{aligned} \tag{17}$$

To compute the next increment, it is necessary only to replace x_0 and y_0 in the above formulas by x_1 and y_1. So, the previously mentioned equations with their boundary condition given in Eq. (14) are altered in terms of initial value problems as stated below (see Ghadikolaei et al. [4]).

$$\begin{aligned} y_1'(\eta) &= y_2 \\ f'(\eta) &= y_1 \\ y_2'(\eta) &= \left(\beta^{-1}(\beta+1)\right)\left\{\left(y_1^2 - (f+g)y_2 - QA_2 e^{-\eta A}\right)/A_1\right\} \\ y_2'(\eta) &= \left(\beta^{-1}(\beta+1)\right)\left\{\left(y_1^2 - (f+g)y_2 - QA_2 e^{-\eta A}\right)/A_1\right\} \end{aligned} \tag{18}$$

$$\begin{aligned} g'(\eta) &= y_3 \\ y_3'(\eta) &= y_4 \\ y_4'(\eta) &= \left(\beta^{-1}(\beta+1)\right)\left\{\left(y_3^2 - (f+g)y_4\right)/A_1\right\} \end{aligned} \tag{19a}$$

$$\theta'(\eta) = y_5 \tag{19b}$$

$$y_5'(\eta) = -\left(\frac{A_3}{A_4 + Rd\left((1+\theta_w)\theta\right)^3}\right)\Pr(f+g)y_5$$

with the boundary conditions

$$\begin{cases} f(0)=0,\ g(0)=0,\ y_1(0)=1, \\ y_3(0)=\alpha \ \text{ and } \ \theta(0)=1 \end{cases} \tag{20}$$

The initial guesstimate was supplied to the unidentified constants $y_2(0)$ i.e., $f''(0)$, $y_4(0)$ i.e., $g''(0)$ and $y_5(0)$ i.e., $\theta'(0)$. Then convenient modification was done on the initial guesstimates to satisfy the boundary conditions $f' \to 0,\ g' \to 0$ and $\theta \to 0$ *as* $\eta \to \infty$. This procedure will be repeated until the convergence criterion of 10^{-8} is reached. In addition, the step size is chosen as $\Delta\eta = 0.001$.

Table 4. Numerical values of the local skin friction coefficient for the base fluid H_2O with Fe_3O_4 and Al_2O_3 for different physical parameters

Parameter	Value	$\left(1+\frac{1}{\beta}\right)\frac{1}{(1-\varphi)^{2.5}}f''(0)$		$\left(1+\frac{1}{\beta}\right)\frac{1}{(1-\varphi)^{2.5}}g''(0)$	
	0.5	-0.981362	-1.031294	-1.011366	-1.069697
A	1.0	-1.009582	-1.058971	-1.088076	-1.145261
	1.5	-1.022133	-1.071264	-1.120831	-1.177502
	0.5	-0.985906	-1.034739	-1.056021	-1.116079
α	1.0	-1.060760	-1.113031	-1.060760	-1.113031
	1.5	-1.129507	-1.184930	-1.042017	-1.091561
	0.05	-1.017985	-1.046576	-1.088062	-1.121237
ϕ	0.10	-1.001493	-1.051042	-1.066391	-1.123907
	0.15	-1.000982	-1.067347	-1.063112	-1.140152
	0.5	-0.763450	-0.816954	-0.493985	-0.559389
Q	1.0	-0.477356	-0.535750	0.180060	0.104759
	1.5	-0.200565	-0.263762	0.823798	0.738718

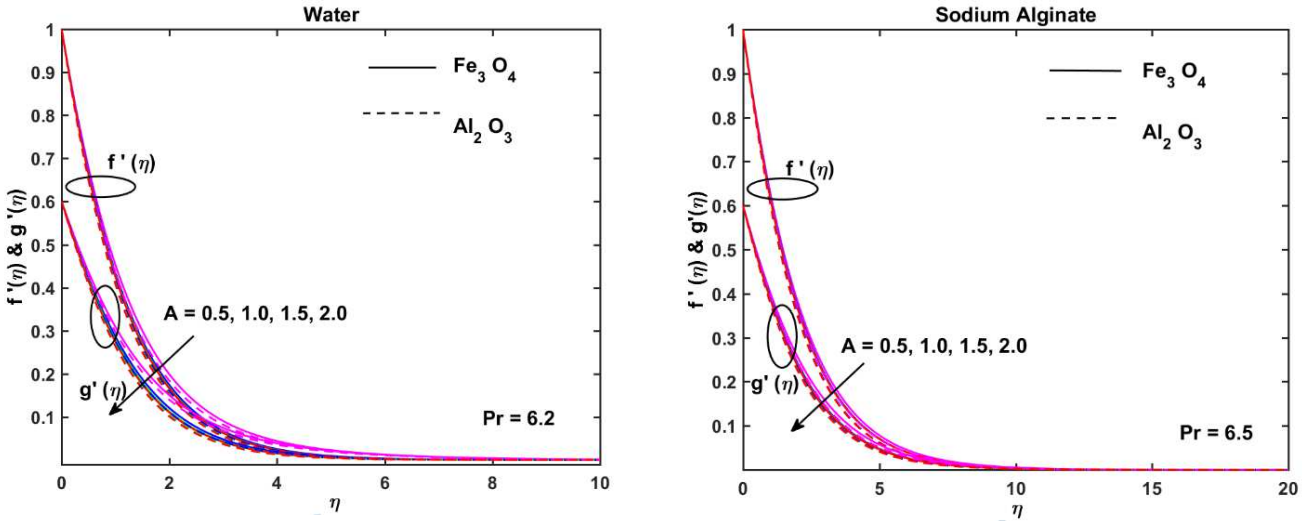

(a) (b)

Fig. 2. Influence of dimensionless parameter A on the velocity profile $f'(\eta)$ for $Q = 0.1, \alpha = 0.6, \theta_w = 1.5,\ Rd = 0.5, \phi = 0.1$

4. Results and Discussion

To get a reasonable understanding of the physical problem numerical calculations have been completed to discuss the impact of various non-dimensional parameters. In order to reach a decision the plots of individual pertinent parameters in different fields are taken into account. The Newtonian base fluid (H_2O) case arises when $\beta \to \infty$. Table 1 records the

thermophysical properties of $H_2O / NaC_6H_9O_7$ base fluids alongside the Fe_3O_4 / Al_2O_3 nanoparticles. Table 2 displays the applied formulation of nanofluids properties. Table 3 portrays the correspondence of the existed consequences of Wang et al. [56], Hayat et al. [55] and Ganesh Kumar et al. [57] with the present outcomes (H_2O base fluid case) with a few special assumptions. This demonstrates the legitimacy of the present outcomes and the precision of the numerical method we utilized as a part of this review. To discover the impression of individual parameters on the common distribution, Figures 1 to 9 are plotted.

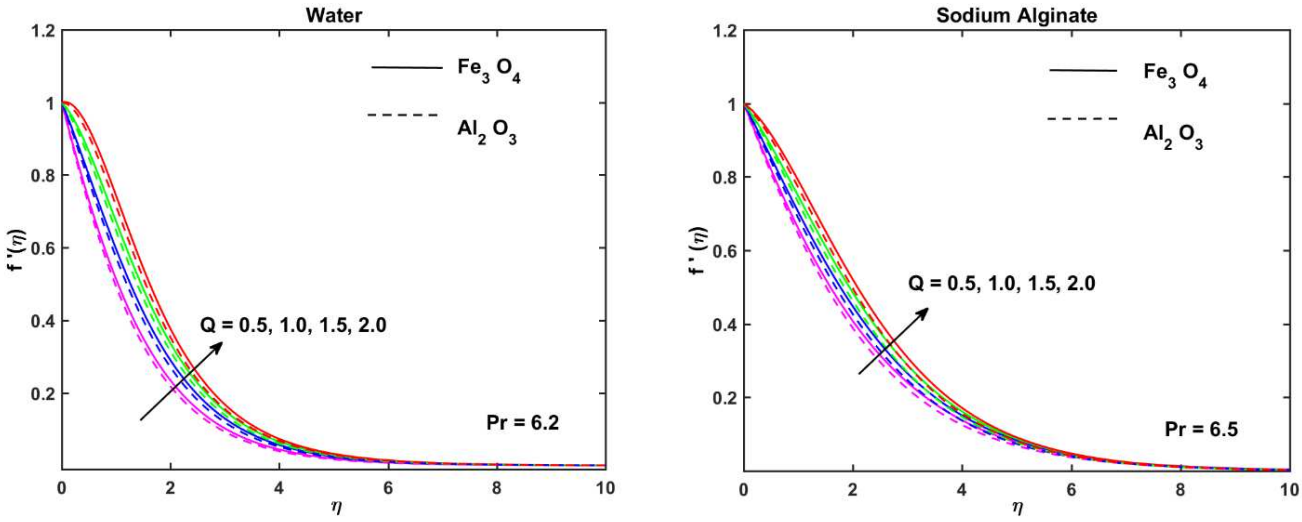

(a) (b)

Fig. 3. Influence of modified Hartman number Q on the velocity profile $\boldsymbol{f'(\eta)}$ for

$$\boldsymbol{A = 0.8, \alpha = 0.6, \theta_w = 1.5, Rd = 0.5, \phi = 0.1}$$

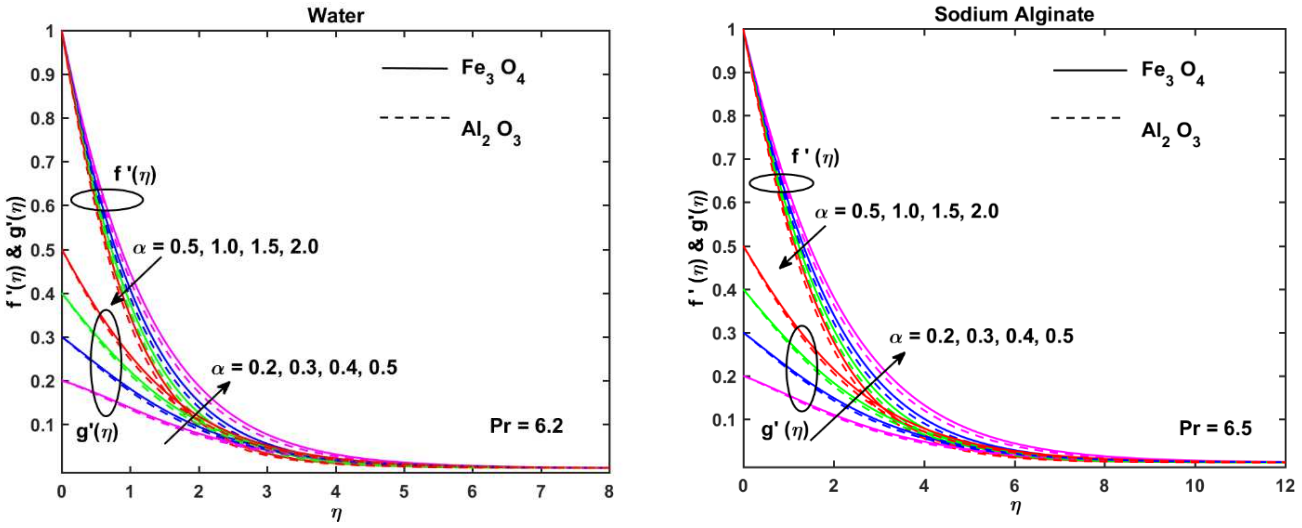

(a) (b)

Fig. 4. Influence of stretching ratio parameter $\boldsymbol{\alpha}$ on the velocity profiles $\boldsymbol{f'(\eta)}$ and $g'(\eta)$ for

$$\boldsymbol{A = 0.8, Q = 0.1, \theta_w = 1.5, Rd = 0.5, \phi = 0.1}$$

4.1. Effects of physical parameters on the velocity & temperature profiles

Figure 2 uncovers the conduct of the velocity distribution $f'(\eta)$ being carried by dimensionless parameter A. It is dissected that velocity distribution demonstrates diminishing conduct for large values of A for selected cases. This is a result of shrinkage in the momentum boundary layer extent. Further, it is noticed that Fe_3O_4 nanoparticles have overwhelming effect of the velocity distribution with the base fluids than Al_2O_3 nanoparticles. Variation of modified Hartmann number Q on the velocity distribution $f'(\eta)$ is portrayed in Figs. 3(a) and 3(b) for both geometries. The higher Q outcomes in magnification of velocity distribution and the relative boundary layer extent. In the way that higher estimations of Q relate to the potency of the external electric field extending above the normal level, heading up in the generation of wall parallel Lorentz force. Subsequently, velocity distribution improves.

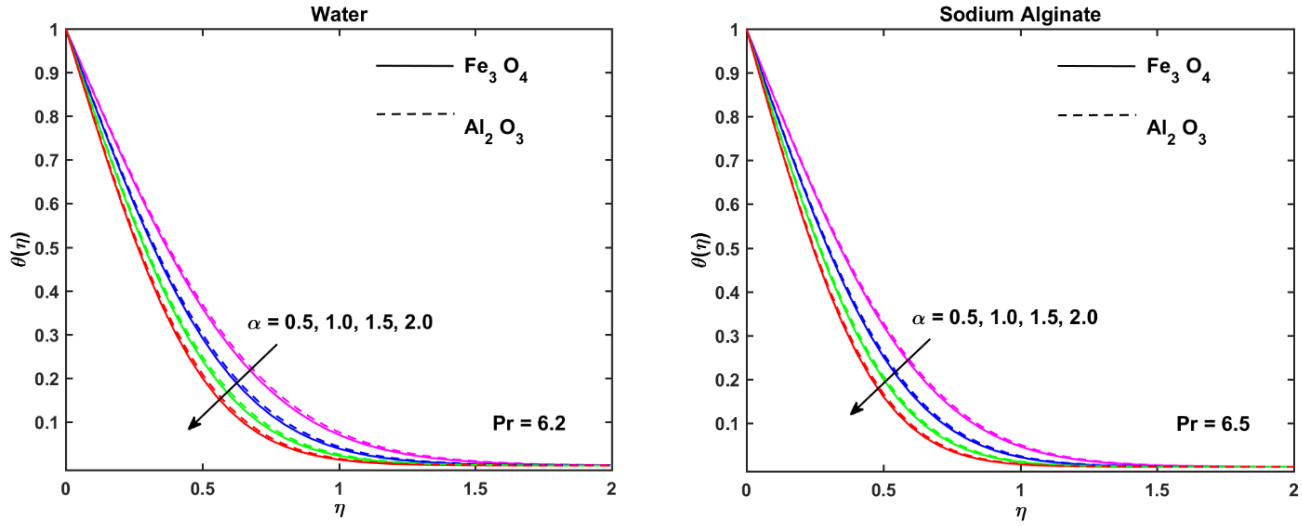

(a) (b)

Fig. 5. Influence of stretching ratio parameter α on the temperature profile for $A = 0.8, Q = 0.1, \theta_w = 1.5, Rd = 0.5, \phi = 0.1$

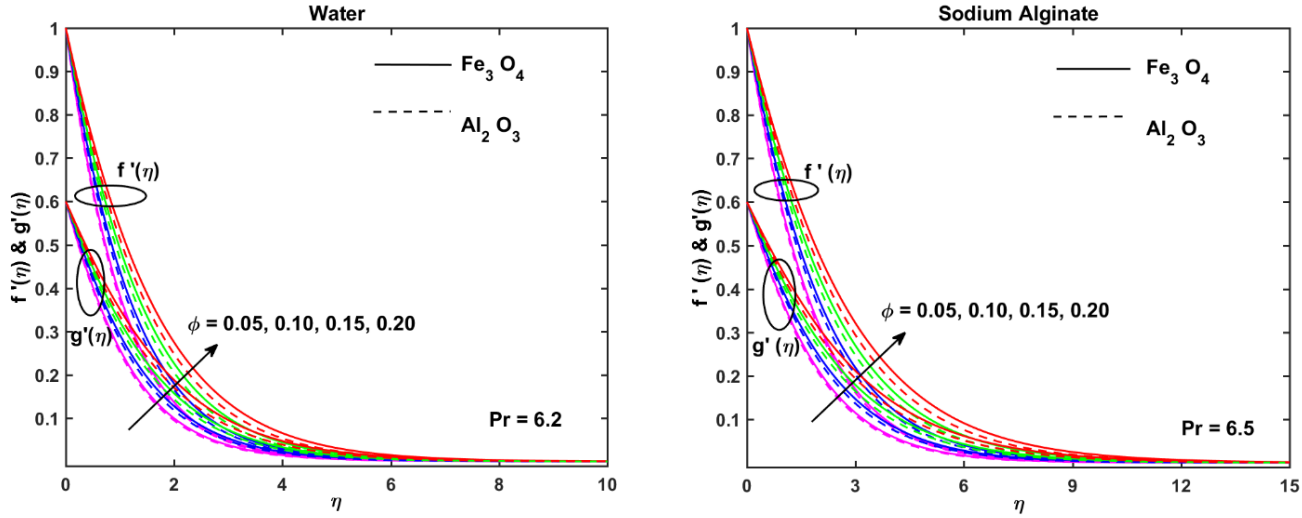

(a) (b)

Fig. 6. Influence of nanoparticle volume fraction parameter ϕ on the velocity profiles $f'(\eta)$ and $g'(\eta)$ for $A = 0.8, \alpha = 0.6, \theta_w = 1.5, Rd = 0.5, Q = 0.1$

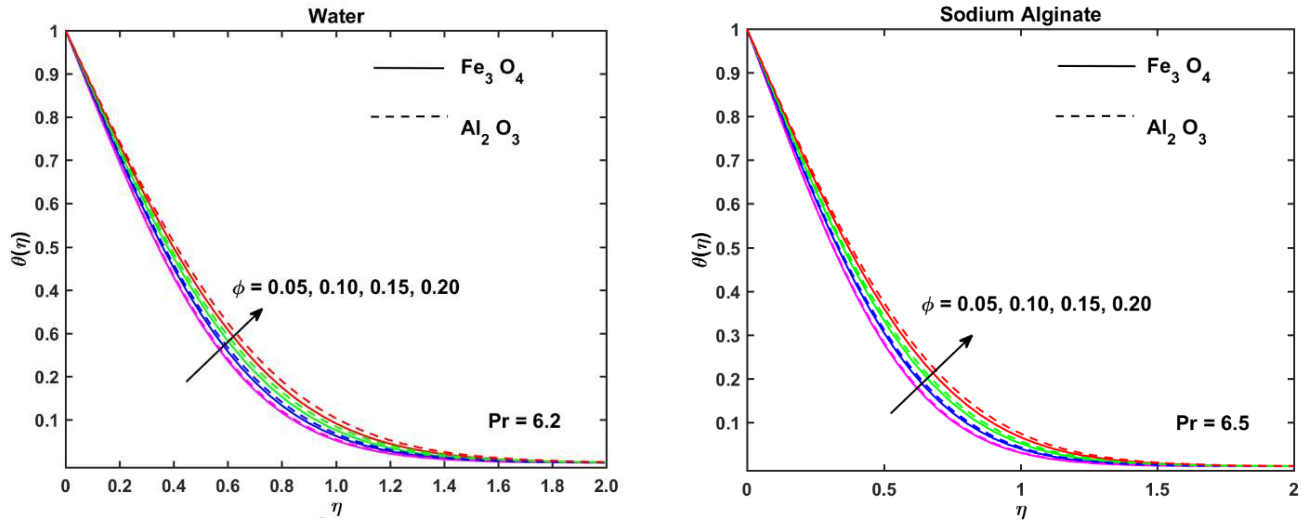

(a) (b)

Fig. 7. Influence of nanoparticle volume fraction parameter ϕ on the temperature profile for $A = 0.8, \alpha = 0.6, \theta_w = 1.5, Rd = 0.5, Q = 0.1$

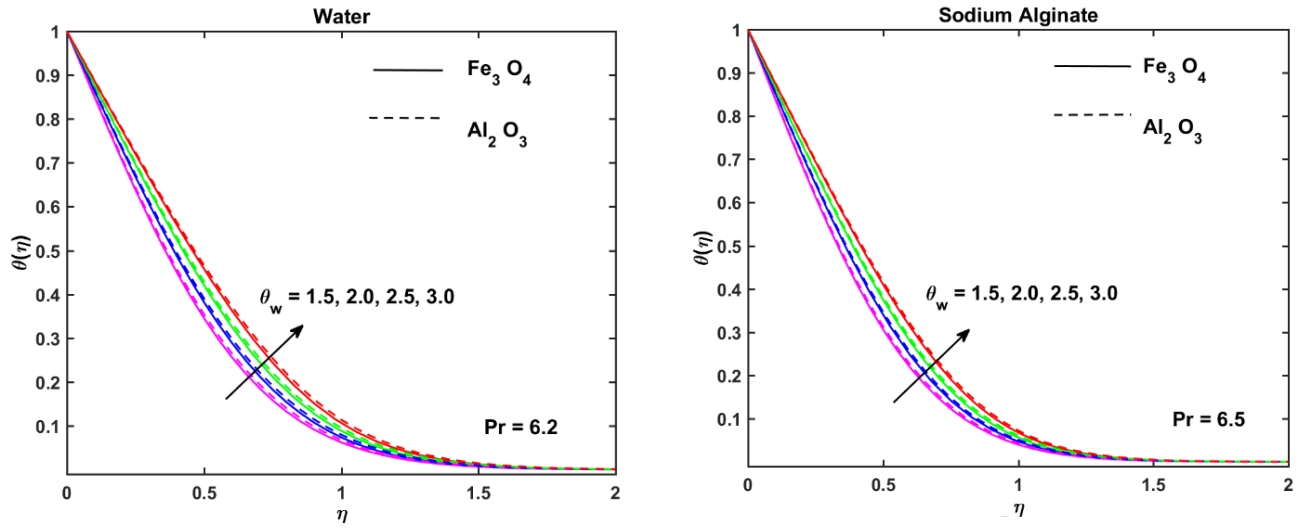

(a) (b)

Fig. 8. Influence of temperature ratio parameter θ_w on the temperature profile for $A = 0.8, \alpha = 0.6, Rd = 0.5, Q = 0.1, \varphi = 0.1$

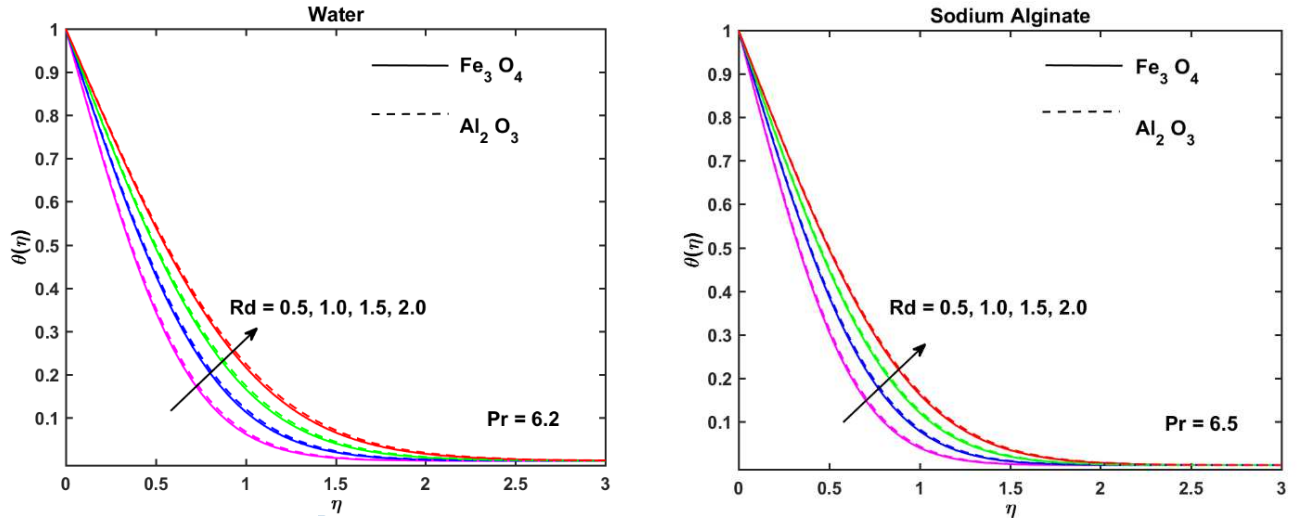

(a) (b)

Fig. 9. Influence of radiation parameter *Rd* on the temperature profile for $A = 0.8, \alpha = 0.6, \theta_w = 1.5, Q = 0.1, \phi = 0.1$

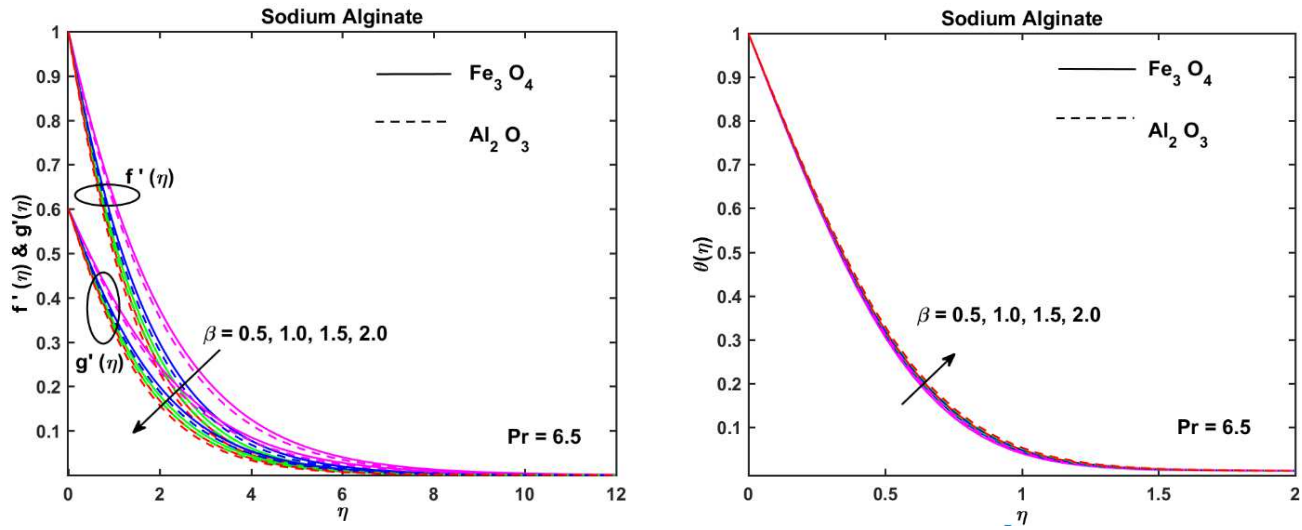

(a) (b)

Fig. 10. Influence of Casson parameter β on the velocity profile and temperature profile for $A = 0.8, \alpha = 0.6, \theta_w = 1.5, Rd = 0.5, Q = 0.1, \phi = 0.1$

Figure 4(a) exhibits the velocity profile $f'(\eta)$ and $g'(\eta)$ of Fe_3O_4 / Al_2O_3 nanoparticles with H_2O for distinct values of stretching ratio parameter α. From this figure, it is seen that an expansion in α prompts to decrease the velocity $f'(\eta)$ along $x-$direction while an inverse tendency can be seen for velocity $g'(\eta)$ along $y-$direction. The ascending values of $\alpha(=b/a)$ initiate an increment in b or deterioration in a. Therefore, along with the $y-$direction the velocity increases and downturns along $x-$direction. Relatively in Fig. 4(b) comparable pattern is observed for $NaC_6H_9O_7$ based nanoparticles. The impact of stretching ratio parameter α is manifested for both cases through Figs 5(a) and 5(b) for $\theta(\eta)$. It is noted that the temperature $\theta(\eta)$ fall off when α top-ups. The potential difference between the hot and cold liquid is matched to the level that is required with augmenting α. Therefore, the thermal boundary, the temperature attenuates.

The feature of ϕ is displayed in Figs. 6(a) and 6(b) on the velocity profiles $f'(\eta)$ and $g'(\eta)$. The velocity profile upturns briskly with the strength of ϕ. For the reason that, as an upward trend in ϕ intensifies, the relative boundary layer extent remarkably, for both cases of nanoparticles and base fluids. Literature proves that the significance of nanofluid is expanding because of their upgraded thermal conductivity. This is a result of the suspension of nanoparticle whose heat conductivity is substantially higher than the base fluids. Clearly higher estimations of ϕ helps advancing the temperature of the nanofluid. These adjustments in the temperature profile are recorded in Fig. 7(a) for H_2O and 7(b) for $NaC_6H_9O_7$ separately.

The temperature ratio parameter showing its potency on $\theta(\eta)$ is manifested for both cases through the Figs 8(a) and 8(b). Under the circumstance $\theta_w > 1$ the temperature curves in the specified domain is higher. θ_w which denotes the temperature at the Riga plate, when extends above relates to the thickening of the temperature boundary layer, which in turn hikes the temperature profile.

Modifying the radiation parameter *Rd,* the corresponding response given by $\theta(\eta)$ is captured in Fig. 9(a) for Fe_3O_4 and Al_2O_3 nanoparticles with H_2O. The temperature profile undergoes natural development by changing *Rd* gradually. The premise is $\partial q_r / \partial z$ which gives measures of the quantity of flux emanating increases which is the primary cause for the thermal growth. Same pattern of the result is given in Fig. 9(b) for Fe_3O_4 and Al_2O_3 nanoparticles with $NaC_6H_9O_7$.

Figure 10(a) gives a clear demonstration of the change of the Casson parameter β on velocity profiles $f'(\eta)$ and $g'(\eta)$. The Casson parameter decreasingly affects $f'(\eta)$ and $g'(\eta)$. This is by reason of a rise in the opposition with increasing β. The temperature curve in Fig. 10(b) indicates an impression produced by the expanding Casson parameter β. Impairing the rate of fluid transport, β, adding strength to the temperature profile.

Table 5. Numerical values of the local skin friction coefficient for the base fluid $NaC_6H_9O_7$ with Fe_3O_4 and Al_2O_3 for different physical parameters

Parameter	Value	$(1+1/\beta)f''(0)/(1-\varphi)^{2.5}$		$(1+1/\beta)g''(0)/(1-\varphi)^{2.5}$	
	0.5	-2.939241	-3.089644	-3.028435	-3.204140
A	1.0	-3.023958	-3.172717	-3.258679	-3.430926
	1.5	-3.061636	-3.209618	-3.356999	-3.527692
	0.5	-2.952982	-3.100070	-3.162233	-3.343140
α	1.0	-3.177210	-3.334653	-3.177210	-3.334653
	1.5	-3.383147	-3.550083	-3.121246	-3.270476
	0.05	-3.051101	-3.137365	-3.260873	-3.360972
ϕ	0.10	-2.999673	-3.148919	-3.193594	-3.366838
	0.15	-2.996651	-3.196283	-3.182024	-3.413775
	0.5	-2.285151	-2.446328	-1.475588	-1.672631
Q	1.0	-1.426380	-1.602311	0.547533	0.320637
	1.5	-0.595529	-0.785946	2.479722	2.223326
	0.5	-2.999673	-3.148919	-3.193594	-3.366838
β	1.0	-2.787272	-2.928769	-2.899565	-3.064561
	1.5	-2.817269	-2.962202	-2.883795	-3.053323

4.2. Effects of physical parameters on the local skin friction coefficients & local Nusselt number

Figures 11(a) and 11(b) are drawn to see the dimensionless parameter A and its impact on $f''(0)$. A out-turn in decrement of $f''(0)$. In addition to what has already been done, the thermal boundary layer thickness also has diminishing behavior for both H_2O and $NaC_6H_9O_7$ nanofluids. The same is seen through $g''(0)$ curves in Fig. 12 for both cases. Figures 13(a) and 13(b) present the change that had undergone various values of stretching ratio parameter α.

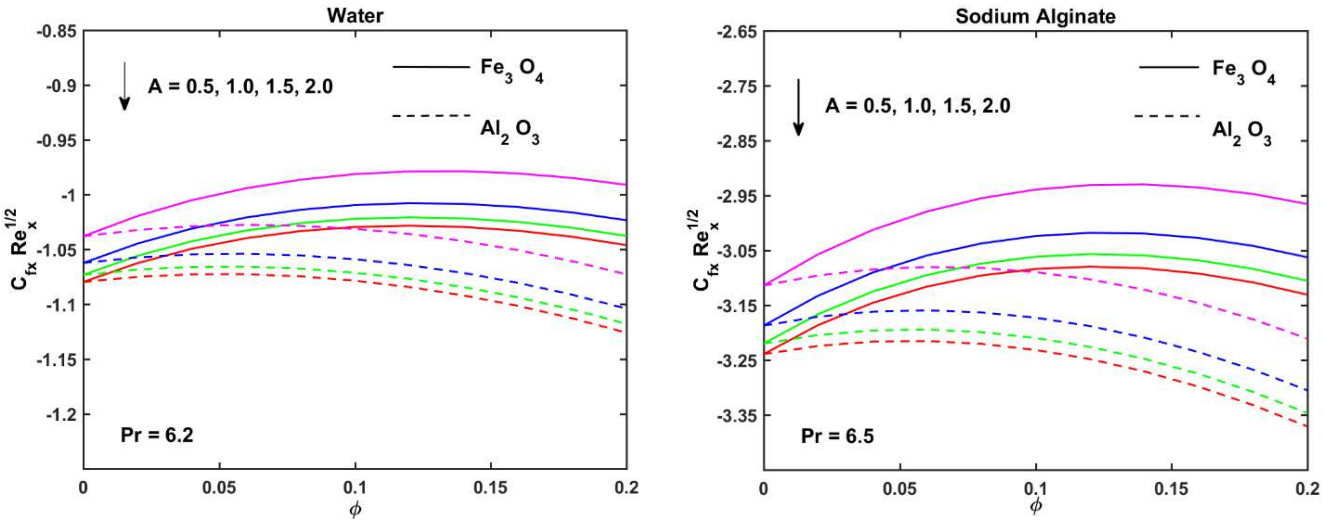

(a) (b)

Fig. 11. Influence of dimensionless parameter A on the local skin friction coefficient in the $x-$ direction for $\alpha = 0.6, \theta_w = 1.5, Rd = 0.5, Q = 0.1, \phi = 0.1$

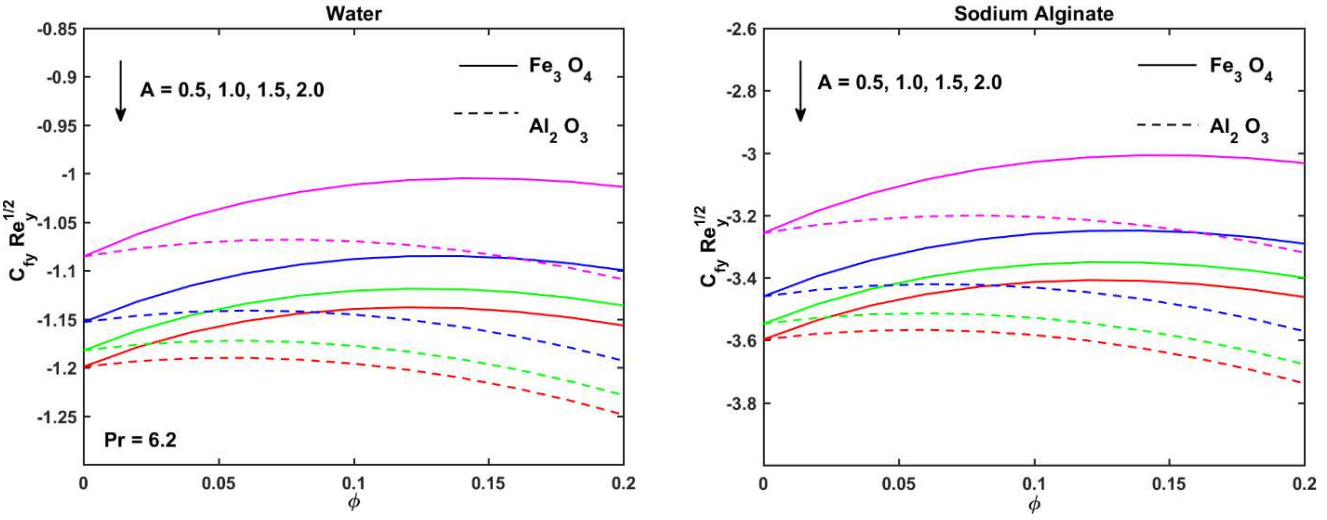

(a) (b)

Fig. 12. Influence of dimensionless parameter A on the local skin friction coefficient in the $y-$ direction for $\alpha = 0.6, \theta_w = 1.5, Rd = 0.5, Q = 0.1, \phi = 0.1$

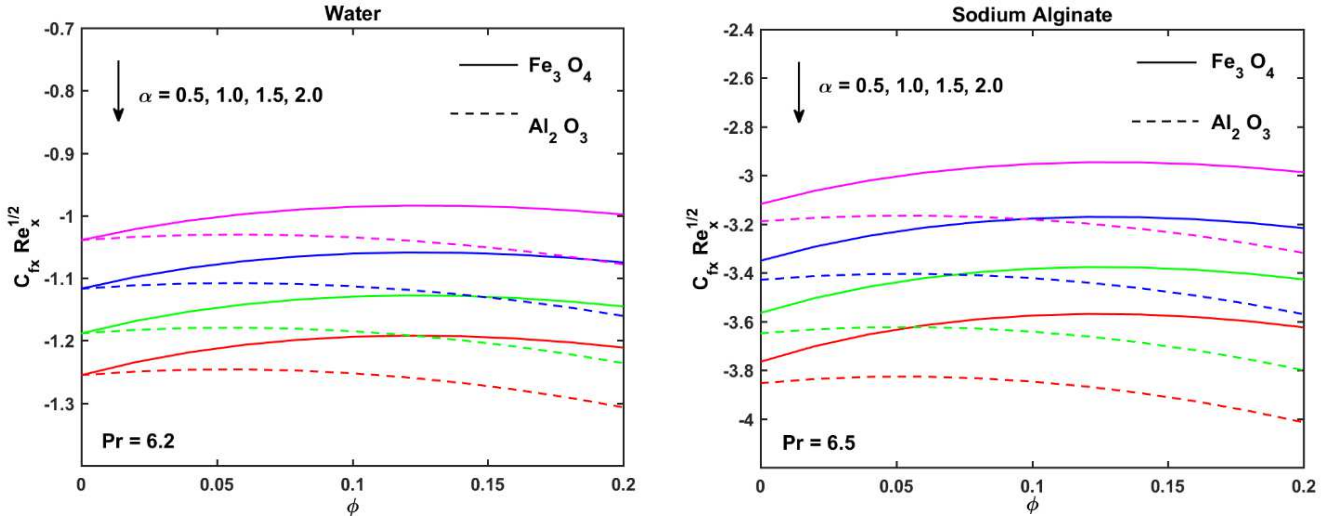

(a) (b)

Fig. 13. Influence of stretching ratio parameter α on the local skin friction coefficient in the $x-$ direction for $A = 0.8, \theta_w = 1.5, Rd = 0.5, Q = 0.1, \phi = 0.1$

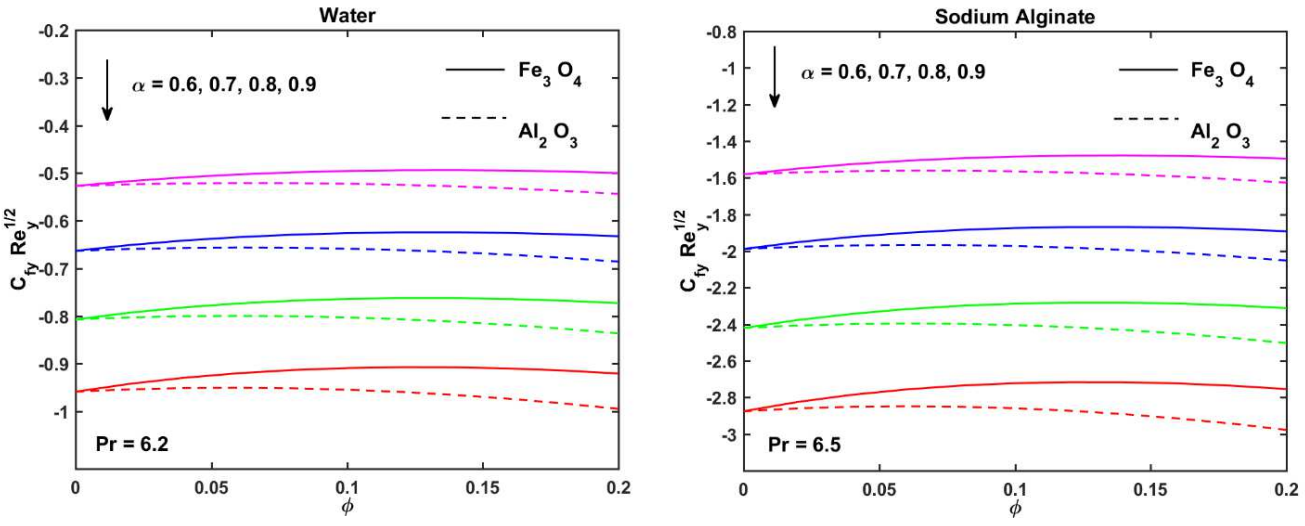

(a) (b)

Fig. 14. Influence of stretching ratio parameter α on the local skin friction coefficient in the y − direction for $A = 0.8, \theta_w = 1.5, Rd = 0.5, Q = 0.1, \phi = 0.1$

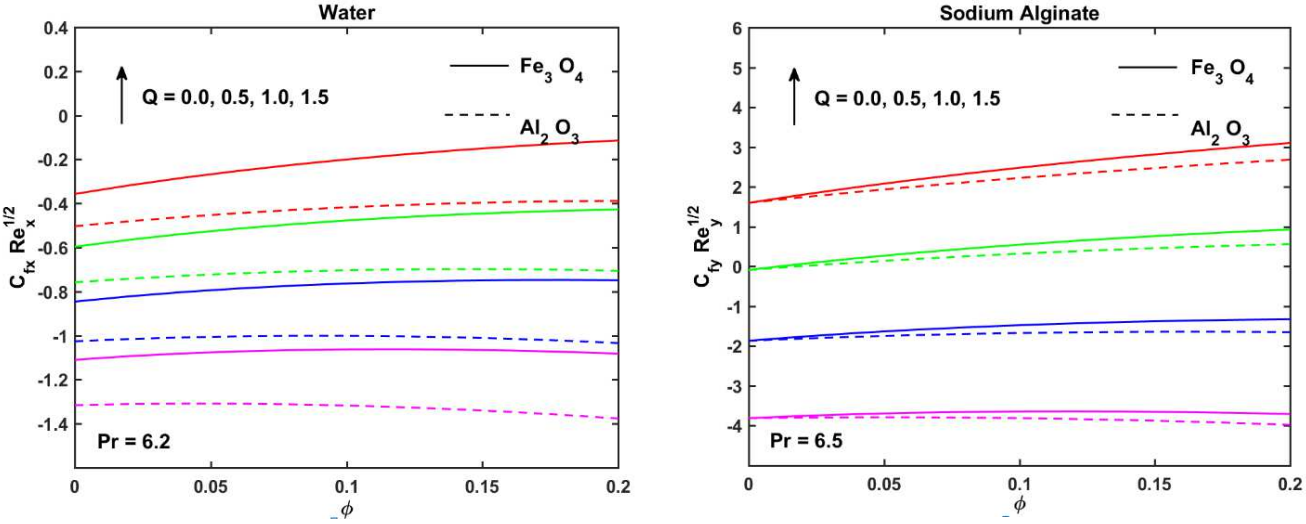

(a) (b)

Fig. 15. Influence of modified Hartman number Q on the local skin friction coefficient in the x − direction for $A = 0.8, \alpha = 0.6, \theta_w = 1.5, Rd = 0.5, \phi = 0.1$

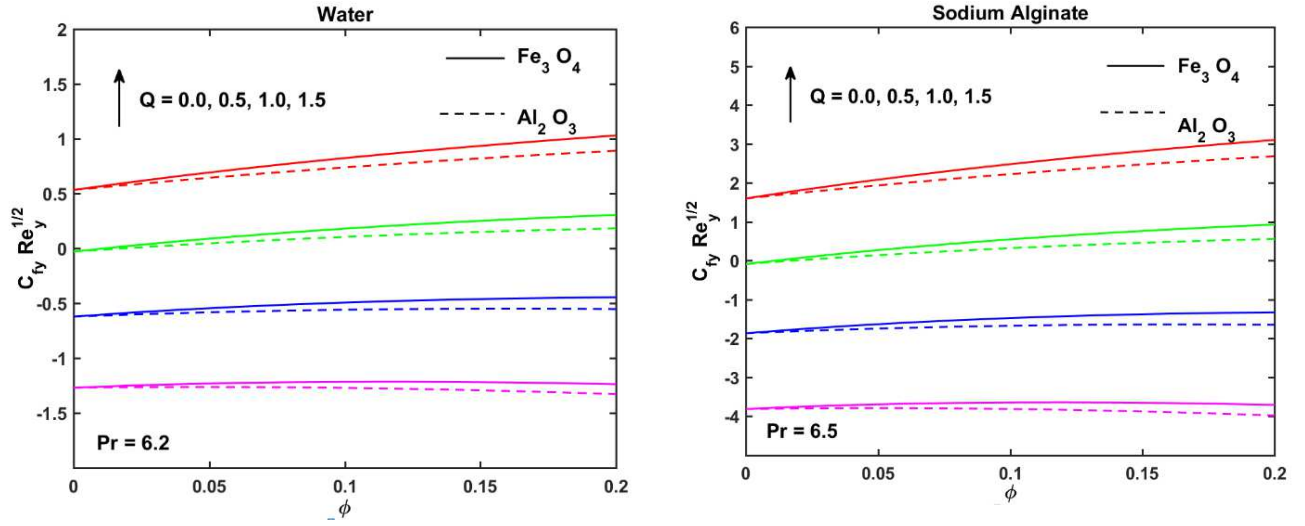

(a) (b)

Fig. 16. Influence of modified Hartman number Q on the local skin friction coefficient in the y − direction for $A = 0.8, \alpha = 0.6, \theta_w = 1.5, Rd = 0.5, \phi = 0.1$

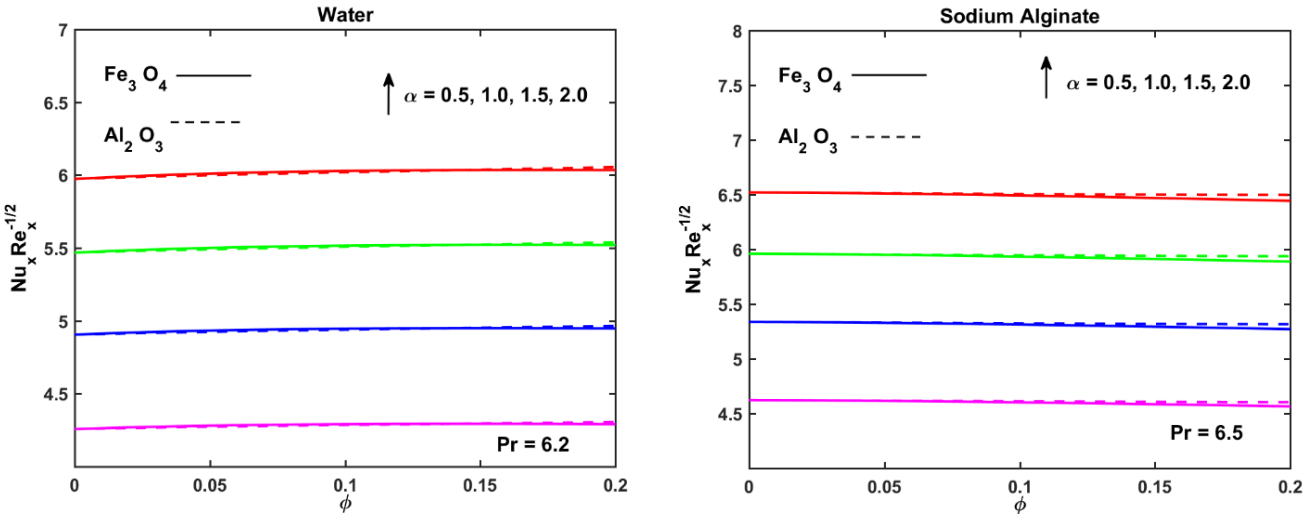

(a) (b)

Fig. 17. Influence of stretching ratio parameter α on the local Nusselt number for $A = 0.8, \theta_w = 1.5, Rd = 0.5, Q = 0.1, \phi = 0.1$

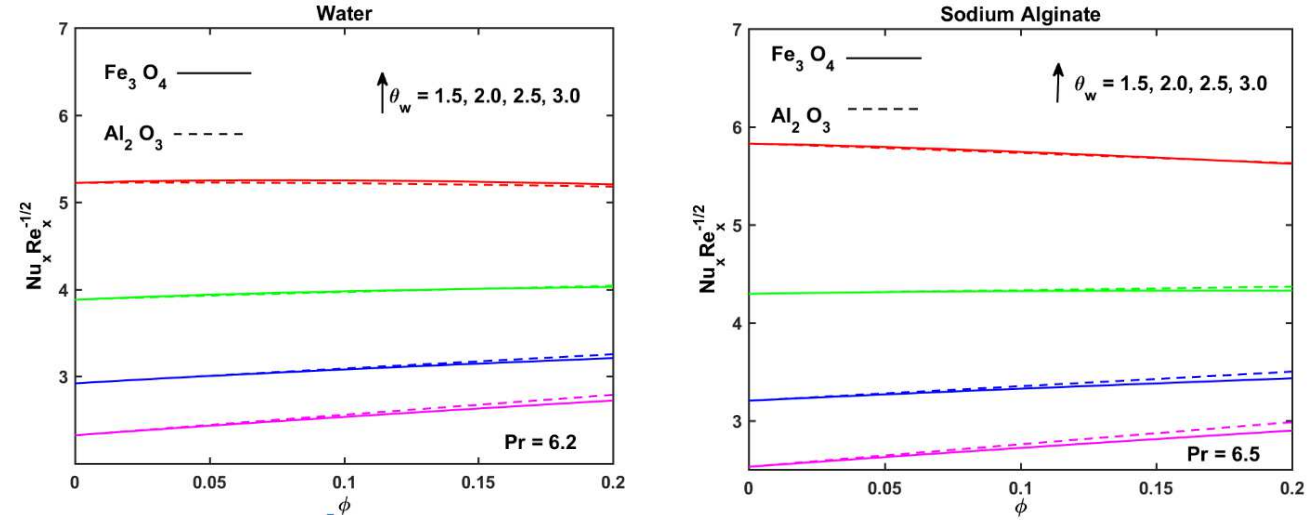

(a) (b)

Fig. 18. Influence of temperature ratio parameter θ_w on the local Nusselt number for $A = 0.8, \alpha = 0.6, Rd = 0.5, Q = 0.1, \phi = 0.1$

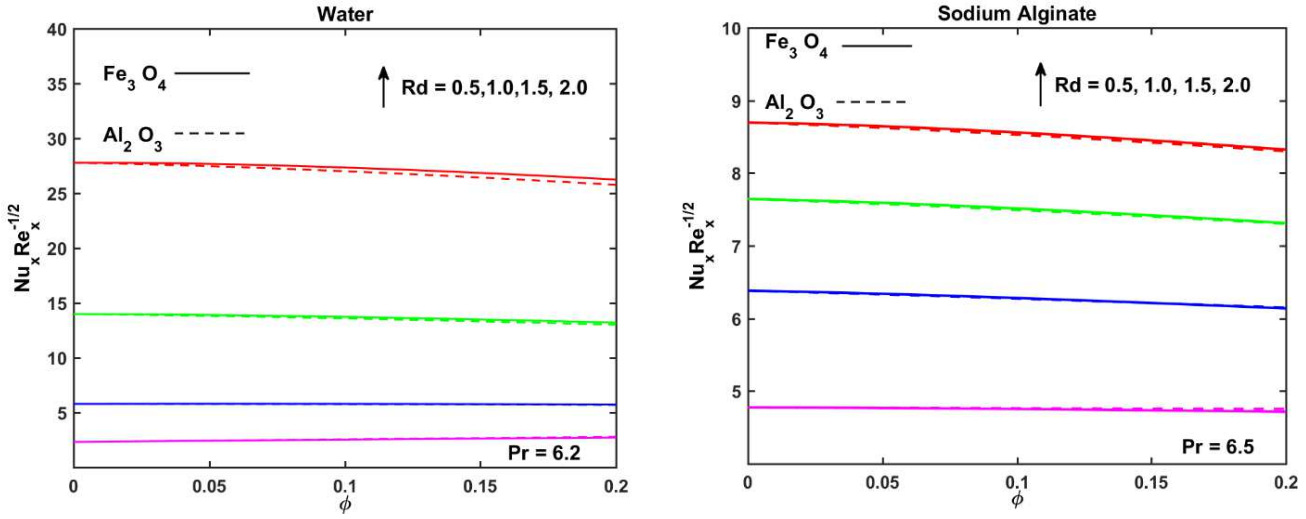

(a) (b)

Fig. 19. Influence of radiation parameter *Rd* on the local Nusselt number for $A = 0.8, \alpha = 0.6, \theta_w = 1.5, Q = 0.1, \phi = 0.1$

On scrutinizing, $f''(0)$ is smaller for large α. Further H_2O based nanofluid has a dominating contribution in comparison to $NaC_6H_9O_7$ based nanofluid. The similar outcome is observed for $g''(0)$ from figures 14(a) and 14(b). Figures 15 and 16 illustrate the effects of modified Hartmann number Q on $f''(0)$ in x-direction and $g''(0)$ in $y-$direction. It is evaluated that the $f''(0)$ and $g''(0)$ increases by advancing Q with ϕ. As stated before (H_2O) based nanofluid show increasing behavior for higher values of Q. In figures 16(a) and 16(b), it is noticed that the expansion in the β prompts an expansion in $f''(0)$ $x-$direction and $g''(0)$ in $y-$direction.

From the aforementioned Figures 11 – 16, we noticed the mixed response of the local skin friction coefficient with respect to ϕ respectively, That is the values of the local skin friction coefficient is higher in the case $\phi < 0.1$whereas gradually decreases for $\phi > 0.1$, as ϕ intensifies the frictional force within the fluid.

Figures 17(a) and 17(b) are drawn to discuss $\theta'(0)$ for various values of stretching ratio parameter α. $\theta'(0)$ seems to face an increment in company with α. The same level of result is noted for distinct values of θ_w and Rd on $\theta'(0)$ in Figs. 18 and 19. The gain in θ_w and Rd encourages to increase the measure of heat transfer.

Tables 4, 5 and 6 are presented with reference to the impacts of relevant parameters on the local skin friction coefficient for both base liquids separately and the local Nusselt number. We observed bring up in the local skin friction coefficient for augmented Q and β. Further, the local Nusselt number is increased for α and Q.

Table 6. Numerical values of the local Nusselt number for $H_2O / NaC_6H_9O_7$ base fluids with Fe_3O_4 / Al_2O_3 for different physical parameters

Parameter	Value	Water		Sodium Alginate	
		Fe_3O_4	Al_2O_3	Fe_3O_4	Al_2O_3
A	0.5	2.516941	2.549671	2.580335	2.615668
	1.0	2.506093	2.538394	2.569573	2.604488
	1.5	2.501542	2.533681	2.565050	2.599800
α	0.5	2.429725	2.461062	2.491164	2.525032
	1.0	2.801933	2.838165	2.872888	2.912044
	1.5	3.126582	3.166849	3.205912	3.249440
ϕ	0.05	2.404015	2.418762	2.465999	2.482015
	0.10	2.509148	2.541565	2.572606	2.607639
	0.15	2.609332	2.661976	2.674093	2.730771
Q	0.5	2.571339	2.605543	2.634785	2.671663
	1.0	2.638257	2.674175	2.701831	2.740493
	1.5	2.697173	2.734485	2.760954	2.801072
β	0.5	-	-	2.572606	2.607639
	1.0	-	-	2.492280	2.519500
	1.5	-	-	2.432949	2.454432
θ_w	1.5	4.431468	4.425297	4.753753	4.763461
	2.0	7.148326	7.095628	7.717226	7.688253
	2.5	11.203872	11.082302	12.175944	12.091922
Rd	0.5	4.431468	4.425297	4.753753	4.763461
	1.0	5.795349	5.765802	6.281627	6.274262
	1.5	6.868885	6.820473	7.514379	7.494764

5. Conclusion

This paper begins to deal with the MHD boundary layer flow and heat transfer of Fe_3O_4 / Al_2O_3 nanoparticles added $H_2O / NaC_6H_9O_7$ base fluids over a Riga plate. The influence of parameters showing different properties on the flow and heat transfer is observed from the plots. Give below are the brief statement of the main points of the discussed study:

- Modified Hartman number M enhances the horizontal velocity $f'(\eta)$ and reduces the temperature profile.
- The temperature ratio parameter θ_w and radiation parameter Rd take part in promoting the temperature profile and measure of heat transport.
- The magnitude of the local skin friction coefficients in both directions increases with an increase in modified Hartmann number Q.
- The rate of heat transfer was found to be higher for the modified Hartmann number Q and stretching ratio parameter α.

- An increase in the values of respective parameters exhibits increment in the local skin friction coefficient of $H_2O - Fe_3O_4$ and increment in the heat transfer rate of $NaC_6H_9O_7 - Al_2O_3$ nanofluid when contrasted with other proposed combinations.

Author Contributions

A.K. Abdul Hakeem and P. Ragupathi contemplated the presented idea. P. Ragupathi and S. Saranya developed the theory and performed the computations. B. Ganga verified the numerical methods and the results that were discussed in the paper. A.K. Abdul Hakeem encouraged P. Ragupathi and S. Saranya to investigate the non-linear radiation aspects and supervised the findings of this work. All authors discussed the results and contributed to the final manuscript.

Conflict of Interest

The authors declared no potential conflicts of interest with respect to the research, authorship and publication of this article.

Funding

The authors received no financial support for the research, authorship and publication of this article.

Nomenclature

A	Material constant
a, b	Constants
a_1	The width of the magnets between the electrodes
C_p	Specific heat coefficient[J/kg.K]
C_f ,C_g	Skin friction coefficients
f , g	Dimensionless stream functions
j_0	Applied current density in electrodes
k^*	Mean absorption coefficient
M_0	Magnetization of the permanent magnets
Nu_x	Local Nusselt number
Pr	Prandtl number of base fluids
p_y	Yield stress of the fluid
Q	Modified Hartmann number
q_w	Wall heat flux [W/m^2]
q_r	Radiative heat flux [W/m^2]
Re_x ,Re_y	Local Reynolds number
T	Local fluid temperature [K]
T_w	Temperature at the surface of the plate [K]
T_∞	Free stream temperature [K]
u_w,v_w	Stretching velocities
u, v, w	Components of velocity [m/s]
x, y, z	Coordinates [m]

Greek Letters

α	Stretching ratio parameter
α_{nf}	Thermal diffusivity of the nanofluid [m^2/s]
β	Casson parameter
ϕ	Volume fraction of nanoparticle
η	Similarity variable
μ	Absolute viscosity [N·s/m^2]
ν	Kinematic viscosity [m^2/s]
σ	Electric conductivity
σ^*	Stefan-Boltzmann constant
ρ	Density [kg/m^3]
ρC_p	Heat capacity [kg/m^3·K]
θ	Dimensionless temperature
θ_w	Temperature ratio parameter
ψ	Stream function
τ	Viscous stress at the surface of the plate [N m^{-2}]

Subscripts

nf	Nanofluid
f	Base fluid
s	Solid nanoparticles
∞	Boundary layer edge

References

[1] Ghadikolaei, S.S., Gholinia, M., and Hoseini, M.E., Natural convection MHD flow due to MoS_2-Ag nanoparticles suspended in $C_2H_6O_2$-H_2O hybrid base fluid with thermal radiation, *Journal of the Taiwan Institute of Chemical Engineers*, 97, 2019, 12 - 23.

[2] Ghadikolaei, S.S., and Gholinia, M., Terrific effect of H_2 on 3D free convection MHD flow of $C_2H_6O_2$-H_2O hybrid base fluid to dissolve *Cu* nanoparticles in a porous space considering the thermal radiation and nanoparticle shapes effects, *International Journal of Hydrogen Energy*, 44(31), 2019, 17072-17083.

[3] Sheikholeslami, M., and Rokni, H.B., Numerical simulation for impact of Coulomb force on nanofluid heat transfer in a porous enclosure in presence of thermal radiation, *International Journal of Heat and Mass Transfer*, 118, 2018, 823-831.

[4] Ghadikolaei, S.S., Hosseinzadeh, K.,Yassari, M., Sadeghi, H., and Ganji, D.D., Boundary layer analysis of micropolar dusty fluid with TiO_2 nanoparticles in a porous medium under the effect of magnetic field and thermal radiation over a stretching sheet, *Journal of Molecular Liquids*, 244, 2017, 374-389.
[5] Li, Z.X., Shahsavar, A., Al-Rashed, A. A.A.A., Kalbasi, R., Afrand, M., and Talebizadehsardari, P., Multi-objective energy and exergy optimization of different configurations of hybrid earth-air heat exchanger and building integrated photovoltaic/thermal system, *Energy Conversion and Management*, 195, 2019, 1098-1110.
[6] Li, Z.X., Al-Rashed, A.A.A., Rostamzadeh, M., Kalbasi, R., Shahsavar, A., and Afrand, M., Heat transfer reduction in buildings by embedding phase change material in multi-layer walls: Effects of repositioning, thermophysical properties and thickness of PCM, *Energy Conversion and Management*, 195, 2019, 43-56.
[7] Li, Z., Sheikholeslami, M., Ayani, M., Shamlooei, M., Shafee, A., Waly, M. I., and Tlili, I., Acceleration of solidification process by means of nanoparticles in an energy storage enclosure using numerical approach, *Physica A: Statistical Mechanics and its Applications*, 524, 2019, 540-552.
[8] Ghadikolaei, S.S., Hosseinzadeh, K., and Ganji, D.D., Numerical study on magnetohydrodynic CNTs-water nanofluids as a micropolar dusty fluid influenced by non-linear thermal radiation and joule heating effect, *Powder Technology*, 340, 2018, 389-399.
[9] Ghadikolaei, S.S., Hosseinzadeh, K., Hatami, M., Ganji, D.D., and Armin, M., Investigation for squeezing flow of ethylene glycol ($C_2H_6O_2$) carbon nanotubes (CNTs) in rotating stretching channel with nonlinear thermal radiation, *Journal of Molecular Liquids*, 263, 2018, 10-21.
[10] Nayak, M. K., Shaw, S., Pandey, V. S., and Chamkha, A. J., Combined effects of slip and convective boundary condition on MHD 3D stretched flow of nanofluid through porous media inspired by non-linear thermal radiation, *Indian Journal of Physics*, 92(8), 2018, 1017-1028.
[11] Saranya, S., Ragupathi, P., Ganga, B., Sharma, R.P., and Abdul Hakeem, A. K., Non-linear radiation effects on magnetic/non-magnetic nanoparticles with different base fluids over a flat plate, *Advanced Powder Technology*, 29, 2018, 1977-1990.
[12] Rehman, F. U., Nadeem, S., Rehman, H. U., and Haq, R. U., Thermophysical analysis for three-dimensional MHD stagnation-point flow of nano-material influenced by an exponential stretching surface, *Results in Physics*, 8, 2018, 316-323.
[13] Mahanthesh, B., Gireesha, B. J., and Gorla, R. S. R., Nanoparticles effect on 3D flow, heat and mass transfer of nanofluid with nonlinear radiation, thermal-diffusion and diffusion-thermo effects, *Journal of Nanofluids*, 5, 2016, 1-10.
[14] Atashafrooz, M., Gandjalikhan Nassab, S. A., and Lari, K., Application of full-spectrum k-distribution method to combined non-gray radiation and forced convection flow in a duct with an expansion, *Journal of Mechanical Science and Technology*, 29(2), 2015, 845-859.
[15] Atashafrooz, M., Gandjalikhan Nassab, S. A., and Lari, K., Numerical analysis of interaction between non-gray radiation and forced convection flow over a recess using the full spectrum k-distribution method, *Heat and Mass Transfer*, 52(2), 2016, 361-377.
[16] Atashafrooz, M., Gandjalikhan Nassab, S. A., and Lari, K., Coupled thermal radiation and mixed convection step flow of nongray gas, *Journal of Heat Transfer*, 138(7), 2016, 072701.
[17] Atashafrooz, M., and Gandjalikhan Nassab, S. A., Combined heat transfer of radiation and forced convection flow of participating gases in a three-dimensional recess, *Journal of Mechanical Science and Technology*, 26(10), 2012, 3357-3368.
[18] Sheikholeslami, M., Sajjadi, H., Amiri Delouei, A., Atashafrooz, M., and Li, Z., Magnetic force and radiation influences on nanofluid transportation through a permeable media considering Al_2O_3 nanoparticles, *Journal of Thermal Analysis and Calorimetry*, 2018, https://doi.org/10.1007/s10973-018-7901-8.
[19] Atashafrooz, M., Effects of Ag-water nanofluid on hydrodynamics and thermal behaviors of three-dimensional separated step flow, *Alexandria Engineering Journal*, 57, 2018, 4277-4285.
[20] Choi, S. U. S., Enhancing thermal conductivity of fluids with nanoparticles, in: D. A. Siginer, H. P. Wang (Eds.), Developments and applications of non-Newtonian flows, 66, ASME FED, 231/MD, 1995, 99 -105.
[21] Buongiorno, J., Convective transport in nanofluids, *ASME Journal of Heat Transfer*, 128, 2006, 240-250.
[22] Sheikholeslami, M., Numerical approach for MHD Al_2O_3-water nanofluid transportation inside a permeable medium using innovative computer method, *Computer Methods in Applied Mechanics and Engineering*, 344, 2019, 306-318.
[23] Hatami, M., Zhou, J., Geng, J., and Jing, D., Variable magnetic field (VMF) effect on the heat transfer of a half-annulus cavity filled by Fe_3O_4-water nanofluid under constant heat flux, *Journal of Magnetism and Magnetic Materials*, 451, 2018, 173-182.
[24] Abdul Hakeem, A. K., Nayak and M. K., Makinde, O. D., Effect of exponentially variable viscosity and permeability on Blasius flow of Carreau nano fluid over an electromagnetic plate through a porous medium, *Journal of Applied and Computational Mechanics*, 5(2), 2019, 390-401.
[25] Sheikholeslami, M., Influence of magnetic field on nanofluid free convection in an open porous cavity by means of Lattice Boltzmann method, *Journal of Molecular Liquids*, 234, 2017, 364-374.
[26] Rashidi, M. M., Vishnu Ganesh, N., Abdul Hakeem, A. K., Ganga, B., and Lorenzini, G., Influences of an effective Prandtl number model on nano boundary layer flow of Al_2O_3-H_2O and Al_2O_3-$C_2H_6O_2$ over a vertical stretching sheet, *International Journal of Heat and Mass Transfer*, 98, 2016, 616-623.
[27] Sheikholeslami, M., Lattice Boltzmann method simulations for MHD non-Darcy nanofluid free convection, *Physica B: Physics of Condensed Matter*, 516, 2017, 55-71

[28] Ghadikolaei, S.S., Hosseinzadeh, K., and Ganji, D.D., MHD raviative boundary layer analysis of micropolar dusty fluid with graphene oxide Go-engine oil nanoparticles in a porous medium over a stretching sheet with joule heating effect, *Powder Technology*, 338, 2018, 425-437.
[29] Ghadikolaei, S.S., Hosseinzadeh, K., and Ganji, D.D., Investigation on ethylene glycol-water mixture fluid suspend by hybrid nanoparticles (TiO_2-CuO) over rotating cone with considering nanoparticles shape factor, *Journal of Molecular Liquids*, 272, 2018, 226-236.
[30] Ghadikolaei, S.S., Yassari, M., Sadeghi, H., Hosseinzadeh, K., and Ganji, D.D., Investigation on thermophysical properties of TiO_2-Cu/H_2O hybrid nanofluid transport dependent on shape factor in MHD stagnation point flow, *Powder Technology*, 322, 2017, 428-438.
[31] Tang, W., Hatami, M., Zhou, J., and Jing, D., Natural convection heat transfer in a nanofluid-filled cavity with double sinusoidal wavy walls of various phase deviations, *International Journal of Heat and Mass Transfer*, 115, 2017, 430-440.
[32] Hatami, M., and Jing, D., Optimization of wavy direct absorber solar collector (WDASC) using Al_2O_3-water nanofluid and RSM analysis, *Applied Thermal Engineering*, 121, 2017, 1040-1050.
[33] Hatami, M., Zhou, J., Geng, J., Song, D., and Jing, D., Optimization of a lid-driven T-shaped porous cavity to improve the nanofluids mixed convection heat transfer, *Journal of Molecular Liquids*, 231, 2017, 620-631.
[34] Pourmehran, O., Rahimi-Gorji, M., Hatami, M., Sahebi, S.A.R., and Domairry, G., Numerical optimization of microchannel heat sink (MCHS) performance cooled by KKL based nanofluids in saturated porous medium, *Journal of the Taiwan Institute of Chemical Engineers*, 55, 2015, 49-68.
[35] Atashafrooz, M., Sheikholeslami, M., Sajjadi, H., and Amiri Delouei, A., Interaction effects of an inclined magnetic field and nanofluid on forced convection heat transfer and flow irreversibility in a duct with an abrupt contraction, *Journal of Magnetism and Magnetic Materials*, 478, 2019, 216-226.
[36] Sajjadi, H., Amiri Delouei, A., Atashafrooz, M., and Sheikholeslami, M., Double MRT Lattice Boltzmann simulation of 3-D MHD natural convection in a cubic cavity with sinusoidal temperature distribution utilizing nanofluid, *International Journal of Heat and Mass Transfer*, 126, 2018, 489-503.
[37] Atashafrooz, M., The effects of buoyancy force on mixed convection heat transfer of MHD nanofluid flow and entropy generation in an inclined duct with separation considering Brownian motion effects, *Journal of Thermal Analysis and Calorimetry*, 2019, https://doi.org/10.1007/s10973-019-08363-w.
[38] Abdul Hakeem, A.K., Ganga, B., Kalaivanan, R., and Renuka, R., Slip effects on Ohmic dissipative non-Newtonian fluid flow in the presence of aligned magnetic field, *Journal of Applied and Computational Mechanics*, DOI: 10.22055/JACM.2019.29024.1543.
[39] Freidoonimehr, N., Rashidi, M. M., Momenpour, M. H., and Rashidi, S., Analytical approximation of heat and mass transfer in MHD non-Newtonian nanofluid flow over a stretching sheet with convective surface boundary conditions, *International Journal of Biomathematics*, 10, 2017, 1750008.
[40] Eid, M.R. and Mahny, K.L., Unsteady MHD heat and mass transfer of a non-Newtonian nanofluid flow of a two-phase model over a permeable stretching wall with heat generation/absorption, *Advanced Powder Technology*, 28(11), 2017, 3063-3073.
[41] Kalaivanan, R., Ganga, B., Ganesh, N.V., and Hakeem, A.K.A., Effect of elastic deformation on nano-second grade fluid flow over a stretching sheet, *Frontiers in Heat and Mass Transfer*, 10, 2018, 20.
[42] Hakeem, A.K.A., Saranya, S., and Ganga, B., Comparative study on Newtonian/non-Newtonian base fluids with magnetic/non-magnetic nanoparticles over a flat plate with uniform heat flux, *Journal of Molecular Liquids*, 230, 2017, 445-452.
[43] Mahanta, G., and Shaw, S., 3D Casson fluid flow past a porous linearly stretching sheet with convective boundary condition, *Alexandria Engineering Journal*, 54, 2015, 653-659.
[44] Butt, A. S., Tufaila, M. N., and Alia, A., Three-dimensional flow of a magnetohydrodynamic Casson fluid over an unsteady stretching sheet embedded into a porous medium, *Journal of Applied Mechanics and Technical Physics*, 57(2), 2016, 283-292.
[45] Shehzad, S. A., Hayat, T., and Alsaedi, A., Three-dimensional MHD flow of Casson fluid in porous medium with heat generation, *Journal of Applied Fluid Mechanics*, 9, 2016, 215-223.
[46] Nadeem, S., Haq, R. U., and Akbar, N. S., MHD three-dimensional boundary layer flow of Casson nanofluid past a linearly stretching sheet with convective boundary condition, *IEEE Transactions on Nanotechnology*, 13(1), 2014, 109-115.
[47] Yousif, M. A., Hatami, M., and Ismael, H. F., Heat transfer analysis of MHD three dimensional Casson fluid flow over a porous stretching sheet by DTM-Pade, *International Journal of Applied and Computational Mathematics*, 3(Suppl 1), 2017, S813-S828.
[48] Gireesha, B. J., Archana, M., Prasannakumara, B. C., Gorla, R. S. R., and Makinde, O. D., MHD three dimensional double diffusive flow of Casson nanofluid with buoyancy forces and nonlinear thermal radiation over a stretching surface, *International Journal of Numerical Methods for Heat & Fluid Flow*, 27(12), 2017, 2858-2878.
[49] Hayat, T., Abbas, T., Ayuba, M., Farooq, M., and Alsaedi, A., Flow of nanofluid due to convectively heated Riga plate with variable thickness, *Journal of Molecular Liquids*, 222, 2016, 854-862.
[50] Ahmad, A., Asghar, S., and Afzal, S., Flow of nanofluid pasta Riga plate, *Journal of Magnetism and Magnetic Materials*, 402, 2016, 44-48.

[51] Abbas, T., Ayub, M., Bhatti, M. M., Rashidi, M. M., and El-Sayed Ali, M., Entropy generation on nanofluid flow through a horizontal Riga plate, *Entropy*, 18(6), 2016, 223.
[52] Hayat, T., Khan, M., Imtiaz, M., and Alsaedi, A., Squeezing flow past a Riga plate with chemical reaction and convective conditions, *Journal of Molecular Liquids*, 225, 2017, 569-576.
[53] Ahmad, R., Mustafa, M., and Turkyilmazoglu, M., Buoyancy effects on nanofluid flow past a convectively heated vertical Riga-plate: A numerical study, *International Journal of Heat and Mass Transfer*, 111, 2017, 827-835.
[54] Mahanthesh, B., Gireesha, B. J., and Gorla, R. S. R., Nonlinear radiative heat transfer in MHD three-dimensional flow of water based nanofluid over a non-linearly stretching sheet with convective boundary condition, *Journal of the Nigerian Mathematical Society*, 35, 2016, 178-198.
[55] Hayat, T., Shehzad, S. A., and Alsaedi, A., Three-dimensional stretched flow of Jeffrey fluid with variable thermal conductivity and thermal radiation, *Advances in Applied Mathematics and Mechanics*, 34(7), 2013, 823-832.
[56] Wang, C. Y., The three-dimensional flow due to a stretching sheet, *Physics of Fluids*, 27, 1984, 1915-1917.
[57] Ganesh Kumar, K., Haq, R. U., Rudraswamy, N. G., and Gireesha, B. J., Effects of mass transfer on MHD three dimensional flow of a Prandtl liquid over a flat plate in the presence of chemical reaction, *Results in Physics*, 7, 2017, 3465-3471.

ORCID iD

A.K. Abdul Hakeem https://orcid.org/0000-0003-1698-7789
P. Ragupathi https://orcid.org/0000-0001-6508-8443
S. Saranya https://orcid.org/0000-0002-4408-1979
B. Ganga https://orcid.org/0000-0003-3742-1696